Microfluidics and Nanofluidics (2024) 28:12
https://doi.org/10.1007/s10404-023-02705-9

RESEARCH

Study on characteristics of microchannel jet for showerhead in different fluid regimes based on hybrid NS-DSMC methodology

Wansuo Liu[1] · Xiangji Yue[1] · Zeng Lin[1]

Received: 12 July 2023 / Accepted: 18 December 2023 / Published online: 15 February 2024

Abstract
The uniformity of the deposition in the plasma-enhanced chemical vapor deposition (PECVD) process is greatly influenced by the uniform effect of the microchannels in the showerhead. Most of the previous studies on showerheads have primarily focused on the axial-direction of microchannels. However, there is a lack of comparative studies on the influence of radial changes and different flow regimes on the flow characteristics of microchannels. In this paper, we utilized the coupling of the Navier–Stokes and Direct Simulation Monte Carlo (NS-DSMC) methods to compare the differences between expansion type microchannels and equal-diameter type microchannels in the slip and transition regimes. The results indicate that in the slip flow regime, the microchannel of equal diameter exhibits a stronger jet compared to the expansion type. However, this situation reverses as the slip flow regime transitions to the transition regime. This reflects the influence of the flow regime on the characteristics of the microchannel and the potential of the combined type to enhance deposition uniformity.

Keywords NS-DSMC method · Transition regime · Showerhead · Microchannel flow · PECVD uniformity

1 Introduction

Plasma-enhanced chemical vapor deposition (PECVD) is a manufacturing process used in film production. Its characteristic is to conduct the plasma combination reaction by ionizing the reaction gas in a rarefied environment and then depositing the product on the surface. Therefore, the uniformity of the gas will directly affect the uniformity of the final deposition on the surface.

To enhance the uniformity of the gas, a showerhead structure is typically incorporated into the reaction chamber. This structure is typically a circular baffle that improves the gas uniformity through the microchannels on it. Lee et al. (2019) studied the distribution of holes in the showerhead, specifically focusing on the influence of the hole open area ratio in the showerhead structure on the film thickness distribution within the wafer. The results indicated that the shape of film deposition could be controlled, and the uniformity of film thickness was improved by optimizing the hole open area ratio of the showerhead structure. In addition, there are other researchers who are focused on studying the structure of holes. Wi et al. (2012) present the characteristics of hydrogenated microcrystalline silicon thin films deposited from a SiH_4/H_2 in the PECVD system equipped with a showerhead. The results show that a higher deposition rate is found in the deep and dense hole region when the shape and density of the holes on the electrode are varied. Xiang et al. (2019) investigated the deposition of a large-area silicon–nitride film using silane and ammonia by PECVD in a 300 mm apparatus with a vertical showerhead. The inherent non-uniformity of films could be improved by utilizing showerheads with holes of different depths. These studies not only demonstrate the influence of hole structure on the uniformity of the showerhead but also examine two types of hole structures: the equal-diameter type and the expansion type. It can be observed that the distribution and structure of holes directly affect the uniformity of the showerhead.

Not only does the structure of the showerhead itself affect uniformity but also the fluid environment can also impact its performance by affecting the flow through the holes. Guensuk et al. studied the Amorphous Carbon Layer (ACL) deposition rate at 733 Pa and 550 ℃, the Knudsen number (*Kn*) is around 0.02181. Moreover, Sung-Suk et al. studied the PECVD reactor at a pressure of 8 torr and a temperature of 200 ℃, and the *Kn* is approximately 0.00132.

✉ Zeng Lin
zlin@mail.neu.edu.cn

[1] School of Mechanical Engineering and Automation, Northeastern University, Shenyang 110819, China

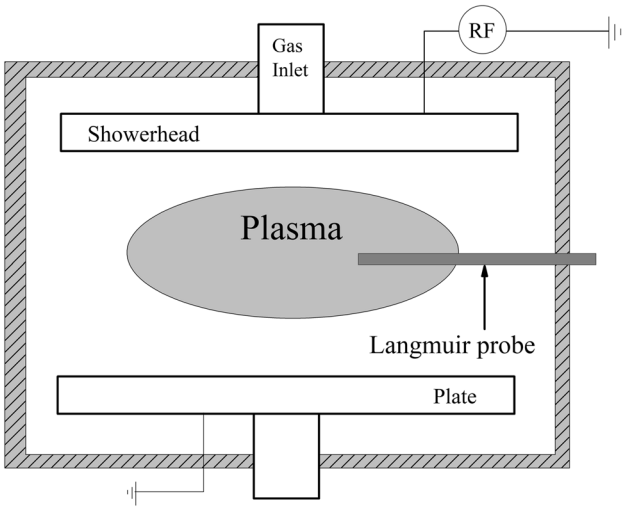

Fig. 1 System of PECVD reaction

Furthermore, Kim and Lee (2017) investigated the structure of a showerhead in a capacitively coupled plasma (CCP) reactor, which utilized an axisymmetric fluid mode in the regime of transition flow. The flow regimes in the above articles are between the slip flow regime and the transition flow regime. From the information in microchannel research (Weng et al. 1999), it is believed that the flow regime would affect the pressure distribution in the microchannel of the showerhead. Therefore, it is necessary to study the influence of rarefied characteristics of the microchannel on the uniformity of the showerhead.

The research on microchannels in rarefied fluids mainly focuses on the distribution of gas pressure, velocity, and temperature within the channel. However, there is a lack of relevant research on jet uniformity. This article focuses on microchannel research and investigates the impact of various microchannel structures and flow regimes on showerhead jet uniformity, by integrating microchannel flow with showerhead uniformity. On one hand, it can enhance research on the flow characteristics of radial structural variations in the microchannel. On the other hand, it can be beneficial in improving the flow uniformity of the showerhead.

2 Experimental procedure

To validate the simulation method used for transition regimes, we conducted experiments to detect plasma using Langmuir probes. The experimental device is shown in Fig. 1. The inner diameter of the vacuum chamber was 340 mm, and the spacing between the upper and lower plates was 60 mm. The gas was injected into the vacuum chamber through the showerhead, and the flow is controlled by the mass flow controller. The upper plate was connected to a radio frequency power source (13.56 MHz) and generated plasma through capacitive coupling. The experimental parameters were set based on the optimal parameters for the oxidation process. The working vacuum was 6.5 Pa, and the radio frequency power was 200 W. The ratio of gas mass flow rate between Ar and O_2 was 1:1, with both gases flowing at a rate of 5 sccm. The Langmuir probe utilized a conventional tungsten probe that was adjusted in position by the drive system. It sweeps the sawtooth waveform with a $\pm$ 110 V output. By using the Langmuir probe, the plasma density can be measured. In this paper, the cross-section of the probe above plate 20 mm was selected for analysis.

3 Numerical method and verification

There are various possibilities for the flow regime in the microchannels of the PECVD chamber. Normally, it will be in the slip flow or transition flow regime. There are significant differences in the calculation methods used for the two flow regimes (Yuan et al. 2020). The continuum flow method that incorporates a slip boundary correction is appropriate for the slip flow regime, but it is not suitable for the transition flow regime. In this paper, a coupled Navier–Stokes and Direct Simulation Monte Carlo (NS-DSMC) method was used to calculate the transition regime. The regions where the continuum flow method is not applicable were determined by calculating the *Kn*. The region would be appropriately expanded and solved using a DSMC method. Thermal radiation is not considered in the calculation, and the heat transfer mechanism between the gas flowing inside the microchannel and the wall is only through molecular interaction. This is because diatomic molecules do not participate in radiant heat exchange under the current rarefied conditions (Huang and Lai 2012).

3.1 The NS method

A three-dimensional model was used for the simulation. The calculation grid adopted a tetrahedral mesh with better adaptability over a wide range, while locally using a hexahedral mesh for higher accuracy. The fundamental governing equations, which include the continuity equation, momentum equation, and energy equation, were discretized using the finite volume method. The inlet pressure was 800 Pa, and the outlet pressure was 667 Pa. The *Kn* was 0.0091–0.0109, and a slip boundary correction was adopted. The tangential momentum accommodation coefficient σ was properly chosen, and the NS solution became in agreement with the experiment when the finite slip velocity was introduced along the microchannel surfaces (Arkilic et al. 1997a; Beskok et al. 1996) given by

$$u_s = u_w + \left(\frac{2-\sigma}{\sigma}\right)\left(\frac{Kn}{1-bKn}\right)\left(\frac{du}{dn}\right)_{wall} \quad (1)$$

where u_s is the dimensionless slip wall velocity, u_w is the dimensionless no-slip wall velocity, σ is the tangential momentum accommodation coefficient, and $\left(\frac{du}{dn}\right)_{wall}$ denotes the normal velocity gradient at the surfaces. The accommodation coefficients $\sigma = 1$ are invoked to model diffuse reflection walls (Rafi et al. 2019). The density-based compressible flow (Gad-el-Hak 1999) and SST turbulence model were adopted. The calculation convergence accuracy is 10^{-4}. The maximum velocity and average pressure were monitored, and the monitoring data reached a stable value before the calculation was completed. The NS method is based on the continuity assumption. However, as the non-continuum effect increases, kinetic theory suggests that the NS equations would become invalid (Fan and Shen 2001).

3.2 The DSMC method

Bird proposed the DSMC method, which is based on statistical methods instead of solving the continuity assumption equation (Bird 1976). The DSMC method describes the state of the system by tracking the positions and velocities of a large number of particles. Each calculated particle in DSMC represents a specific number of real particles. Through grid division, the motion state of particles in each grid area can be calculated to represent the flow state of the grid area.

Based on the open-source OpenFOAM software, the rarefied fluid was simulated using the dsmcFoam module with the DSMC method (Palharini et al. 2015). The molecular free path (λ) was calculated as

$$\lambda = \left(\frac{2(5-2\omega)(7-2\omega)}{15}\right)\left(\frac{\mu}{\rho}\right)\left(\frac{m}{2\pi kT}\right)^{1/2} \quad (2)$$

where ω is the temperature coefficient of viscosity, m is the atomic mass, k is the Boltzmann constant, T is the temperature, μ is the gas dynamic viscosity, and ρ is the gas density. Ensuring that the mesh size was a fraction of the free path (Cai et al. 2022), the time-step size was a fraction of the average collision time, and the average number of particles per cell was 25 (Ghazanfari et al. 2022; Scanlon et al. 2010). A variable hard sphere (VHS) collision model was used (Rafi et al. 2019; Moss and Price 1997). The Maxwell wall condition, which is suitable for rarefied flow interaction, was used (Virgile et al. 2022). The computational efficiency of the DSMC method depends on the number of particles, which in turn is related to the free path. Therefore, the DSMC method is mostly used to solve the non-continuum regime of the flow field.

3.3 The slip flow method verification

In the slip flow simulation, the FLUENT calculation module in ANSYS software was used for the simulation. The accuracy of the microchannel jet calculation is verified by comparing it with other scholars' research.

Beskok et al. (1996) studied the combined effects of compressibility and rarefaction in gas microfluidics in slip flow structures with *Kn* less than 0.3. Arkilic et al. (1997b) proposed an analytical solution for the pressure distribution in microchannels based on a first-order slip boundary condition model. The models of ARKILIC et al. and BESKOK et al. demonstrate that compressibility can lead to non-linear pressure distributions. In previous studies (Huang and Lai 2012; Jang and Wereley 2004; Ko and Gau 2011; Pong et al. 1994; Zohar et al. 2002), it was shown that the pressure distribution in microchannels exhibits non-linear behavior, which is expressed as $S_{\text{non-linear}}$. The formula for calculating the dimensionless non-linearity is defined as:

$$non-linearity = \frac{S_{non-linear}}{S_{base}} \quad (3)$$

where $S_{\text{non-linear}} = \int_0^L (P(x) - P_{linear}(x))dx$, $S_{base} = (P_{in} - P_{out})L/2$. Considering the fluid's thinness, Gao et al. (2018) modified formula (3) to:

$$\text{non-linearity}_{(Kn=0)} = \frac{1}{3} - \frac{2}{3\left(\sqrt{1+\frac{32Lc^2Ma^2}{TRr_0Re}}+1\right)} \quad (4)$$

where L is the pipe length, c is the pipe flow velocity, Ma is the Mach number, T is the temperature, R and r_0 are the viscosity coefficients, and Re is the Reynolds number. It is shown that for a given gas type and microchannel, the non-linearity in the continuum flow region depends on Ma and Re. In order to study the characteristics of microtube flow more succinctly, the pressure ratio (η) is utilized to simplify formula (4). Because η has considered the influence of Ma and Re on non-linearity. Gao et al. provided a simplified formula as follows:

$$non-linearity_{(Kn=0)} = \frac{1}{3} - \frac{2}{3(\eta+1)} \quad (5)$$

Formula (5) shows that non-linearity is the only effect of pressure ratio in the continuum flow regime. The non-linearity increases with the increase of η. When η approaches infinity, it can reach the maximum limit of non-linearity (33%). When η approaches 1, the non-linearity becomes 0, and the compressibility of the fluid disappears.

Weng et al. (1999) normalized the flow field values in their study of microchannel flow, as shown in Fig. 2a. In this figure, D_0 represents the inverse Knudsen number ($D_0 = \frac{2r}{\sqrt{\pi}\lambda}$). Figure 2a shows the non-linear characteristics

under different pressure ratios and rarefaction. It demonstrates that the non-linearity decreases as the pressure ratio decreases. Comparing our simulation data with Fig. 2b, it can be seen that the non-linear characteristics of our simulation results are consistent with the research findings of WENG et al.

The analysis results of Gao et al. (2018), Huang and Lai (2012), Jang and Wereley (2004), and Pong et al. (1994) are compared, as shown in Fig. 3. The range of *Kn* studied includes slip flows. GAO et al. studied a range of 0.02–6.6, Huang et al. studied a range of 0.0015–0.014, Jang et al. studied a range of 0–0.104, and PONG et al. studied a range of 0–0.155. The analysis results of Huang et al., Jang et al., and Pong et al. are very consistent with the formula (5) provided by Gao et al. In $\eta = 1.2$, the non-linear result of formula (5) is 3%, while our simulation result is 4.53%. The simulation result is consistent with the previous findings.

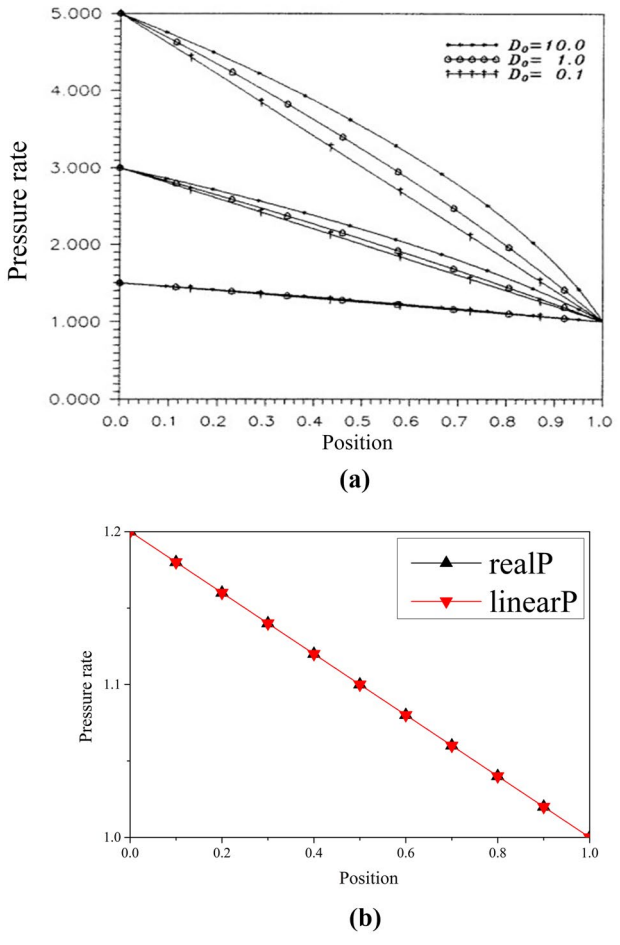

Fig. 2 Relative outlet pressure distribution curves, **a** Pressure curves of different inverse Knudsen numbers and pressure ratios (Weng et al. 1999), **b** Pressure ratio 1.2 pressure curves

3.4 The transition flow simulation method and verification

In the case of an inlet pressure of 8.35 Pa and an outlet pressure of 6.5 Pa, the *Kn* value ranged from 0.0025 to 1.12. The flow field in the PECVD chamber was primarily in the laminar continuum flow regime, whereas the gas in the 0.8 mm diameter microchannel was in the transition flow regime (Aktas et al. 2001). We adopt the NS-DSMC coupling algorithm to solve this multi-flow regime problem. The NS-DSMC coupling method is based on the open-source OpenFOAM software. A steady-state solver called rhoSimpleFoam was used in the continuum flow regime. Rarefied regimes in the microchannel flow field were solved using the DSMC procedure in the dsmcFoam module.

The DSMC method has a high computational accuracy (Wagner 1992), but the disadvantage is that it requires a large number of computational resources in the continuum regime. The NS method also exhibits high reliability specifically for the continuum domain. Therefore, we established the coupling of NS and DSMC methods to solve different regions. Our coupling method did not modify the two modules; instead, it facilitated interaction between two excellent algorithms at an appropriate position. We believe that the key issue to be solved by the coupling method is not computational accuracy, but computational efficiency. Therefore, we compared the results of the NS-DSMC method with those of the DSMC method in order to achieve the same level of accuracy but with higher computational efficiency.

First of all, the statistical scatter calculated by DSMC will only cause numerical fluctuations of the boundary grids but will have little effect on the internal grids. Therefore, the overlapping grid method can be used to transfer internal data for coupling (Schwartzentruber and Boyd 2006). The DSMC region was extended into the NS region to create an overlapping region. The coupling process must be carried

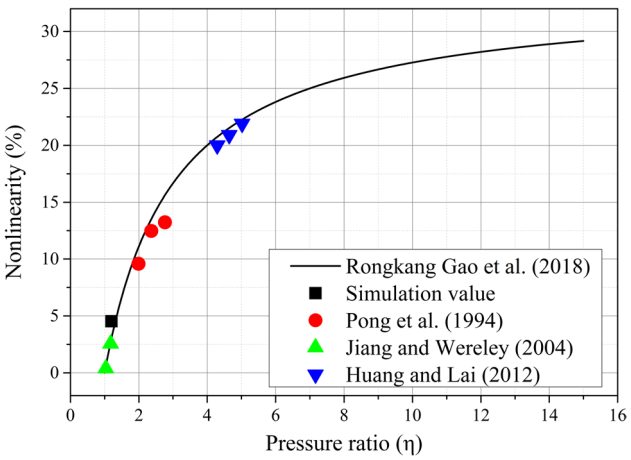

Fig. 3 Comparison of calculation and experimental results

out in the continuum domain in order to smoothly transition the program from the particle domain simulation to the continuum domain (Eggers and Beylich 1994). The size of the overlapping grid has little effect on the results (Aktas and Aluru 2002), and its purpose is to transfer the internally stable solution of DSMC and ensure the validity of the NS method in the coupled region. Therefore, we extend the DSMC area to the NS area, as shown in Fig. 4.

Second, a state-based coupling approach is adopted (Roveda et al. 1998, 2000; Farber et al. 2016). Boundary conditions are imposed on rarefied gas molecular simulations using Chapman-Enskog velocity distributions (Aktas and Aluru 2002). Compared to the boundary conditions of the Maxwellian distribution, the Chapman-Enskog distribution is better suited for boundary conditions that are close to the equilibrium region (Schwartzentruber and Boyd 2006). The flow velocities of simulated molecules into DSMC boundary cells are obtained from the Chapman-Enskog velocity distribution function, which is based on macroscopic flow variables.

Furthermore, by adopting the sub-relaxation technique, the statistical errors in DSMC can be effectively reduced (Sun and Boyd 2005). Both the sub-relaxation technique and the overlapping grid are used to transfer the stable results of the DSMC domain to the NS domain. The overlapping grid and the Chapman-Enskog distribution are used to exchange boundary conditions between continuum domains and molecular domains (John and Damodaran 2009).

Also, we adopted a two-way coupling method instead of the traditional one-way coupling method (Rafi et al. 2019; Virgile et al. 2022). Normally, the NS-DSMC method is calculated using the NS method and then handing over the larger *Kn* domain to the DSMC method. The data is one-way from NS to DSMC. We applied the two-way method to feed the DSMC method data back to the NS method, both of which would evolve simultaneously. The comparison results between one-way and two-way coupling are shown in Fig. 5,

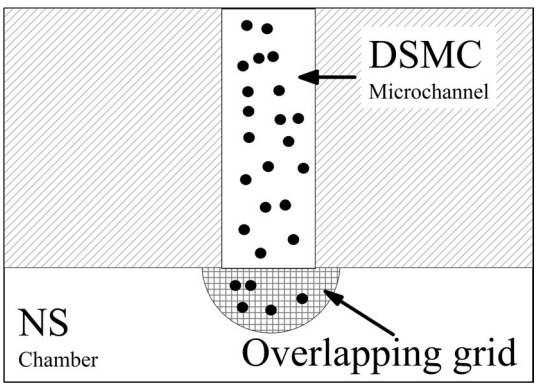

Fig. 4 Schematic diagram of calculation area division

which indicate that the two-way coupling method achieved higher efficiency and accuracy.

Finally, the time decoupling of the steady-state coupling process is achieved by employing the Schwarz alternation method. By adopting the serial Schwarz alternation method, the exchange of subdomain steady-state solutions is realized, allowing for the evolution of the entire flow field. Using the Schwarz alternation method and Dirichlet-Dirichlet boundary conditions, the location of the solver interface for the two domains is pre-specified to facilitate data exchange. This method is suitable for coupled low-speed steady-state problems, and the implicit iterative coupling method is used to avoid the issue of explicit integration to the global steady-state (Aktas and Aluru 2002).

In Fig. 6, NS-DSMC (NS) represents the calculation result of the NS subdomain in the coupling method, and similarly NS-DSMC (DSMC) is the result of the DSMC subdomain. The results showed that the NS-DSMC results were

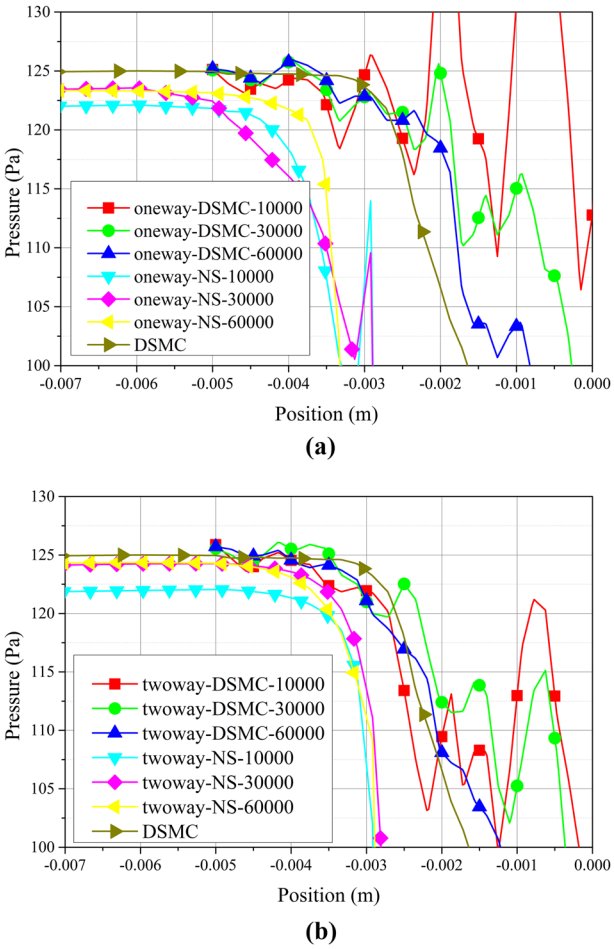

Fig. 5 Comparison of 10,000–60000 calculation step result curves between one-way coupling and two-way coupling at the inlet position of the microchannel, **a** one-way coupling method, **b** two-way coupling method

highly consistent with the DSMC results which illustrate that the coupling method has been completed. The electron density obtained from Langmuir probe detection equipment and the flow field velocity calculated using the NS-DSMC method are shown in Fig. 7. The cross-sectional position is situated in the middle of the chamber. The position of 0.00 m represents the center of the chamber, and the position of -0.10 m indicates the edge of the chamber. It can be seen that the results of the NS-DSMC method are consistent with the experimental results, which aligns with the findings of Yambe et al. (Yambe et al. 2014).

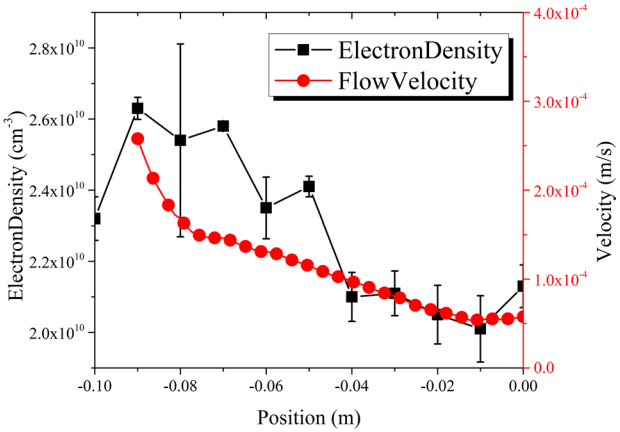

Fig. 7 Comparison of electron density and velocity calculated by NS-DSMC method

4 Results and discussion

The microchannel and chamber geometry studied in this article are shown in Fig. 8. The coordinate system uses the vertical direction (gas flow direction) as the z-axis and the horizontal direction (radial direction) as the x and y axes. The coordinate origin is the center of the outlet of the microchannel, situated at the center of the chamber.

In the slip flow regime situation, as shown in Fig. 9a, b, the equal-diameter type had a stronger jet, and the axial velocity of the equal-diameter type was higher than that of the expansion type. The results in Fig. 9b is in the middle line of the microchannels in Fig. 9a. In the transition regime situation, the characteristics of the jet were inverted for the two types of microchannels. As shown in Fig. 9c, the line out of the microchannel labeled as "z 0.0015" indicates a distance of 0.0015 m from the outlet. The equal-diameter type had a higher velocity than the expansion type, but the situation changed at "z 0.004" where the expansion type had a higher velocity. The velocity distribution exhibits a significant disparity between the slip flow regime and the transition flow regime. Figure 9a and c have different velocity magnitudes, mainly due to calculations performed under two different pressures. This does not affect the conclusion. Although (a) and (c) have different pressures and velocities, we are comparing the performance of the equal-diameter type and expansion type under the same conditions, i.e., (a) or (c). It needs to be explained here that the reason why the pressure is not adjusted to make the flow rate level consistent is because the pressure environment used is the continuum pressure and transition flow pressure that will appear in actual production.

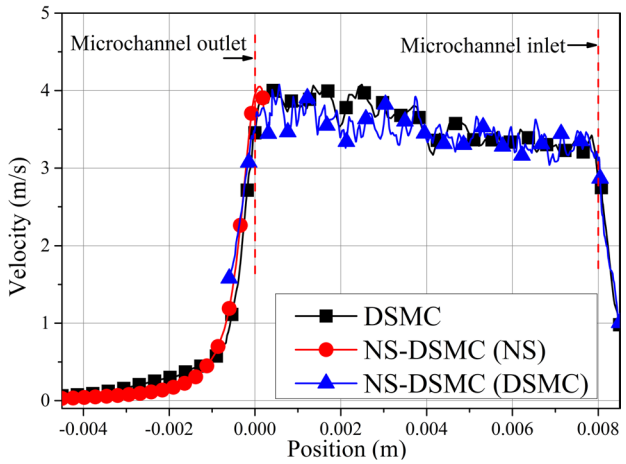

Fig. 6 Comparison of NS-DSMC and DSMC result curves of microchannel flow field

First, the difference between transition flow and slip flow can be analyzed by examining the pressure in the microchannel. As shown in Fig. 10, the pressure evolution was smoother for the transition regime in the microchannel. The pressure in the slip flow regime significantly decreased at the outlet. This means that the fluid consumed more energy to expand in the outlet, resulting in the formation of a high-velocity jet of the equal-diameter type. In addition, the area around the outlet would form vortices to stabilize the jet, which resulted in the equal-diameter type producing a stronger jet than the expansion type in the slip flow regime.

The difference in jet behavior between slip flow and transition flow for equal-diameter types is analyzed above. After that, the difference between the equal-diameter type and expansion type in the transition regime is shown in Fig. 11. The figure illustrates the velocity distribution in the horizontal direction. The equal-diameter type has a high horizontal velocity, indicating that the flow energy is expended in the horizontal direction. The fluid expanded differently for the expansion type and equal-diameter type microchannels. For the expansion type, the fluid would expand within the conical cavity. The direction of fluid energy diffusion was primarily focused on the vertical direction due to the constraints imposed by the walls. By comparison, the diffusion

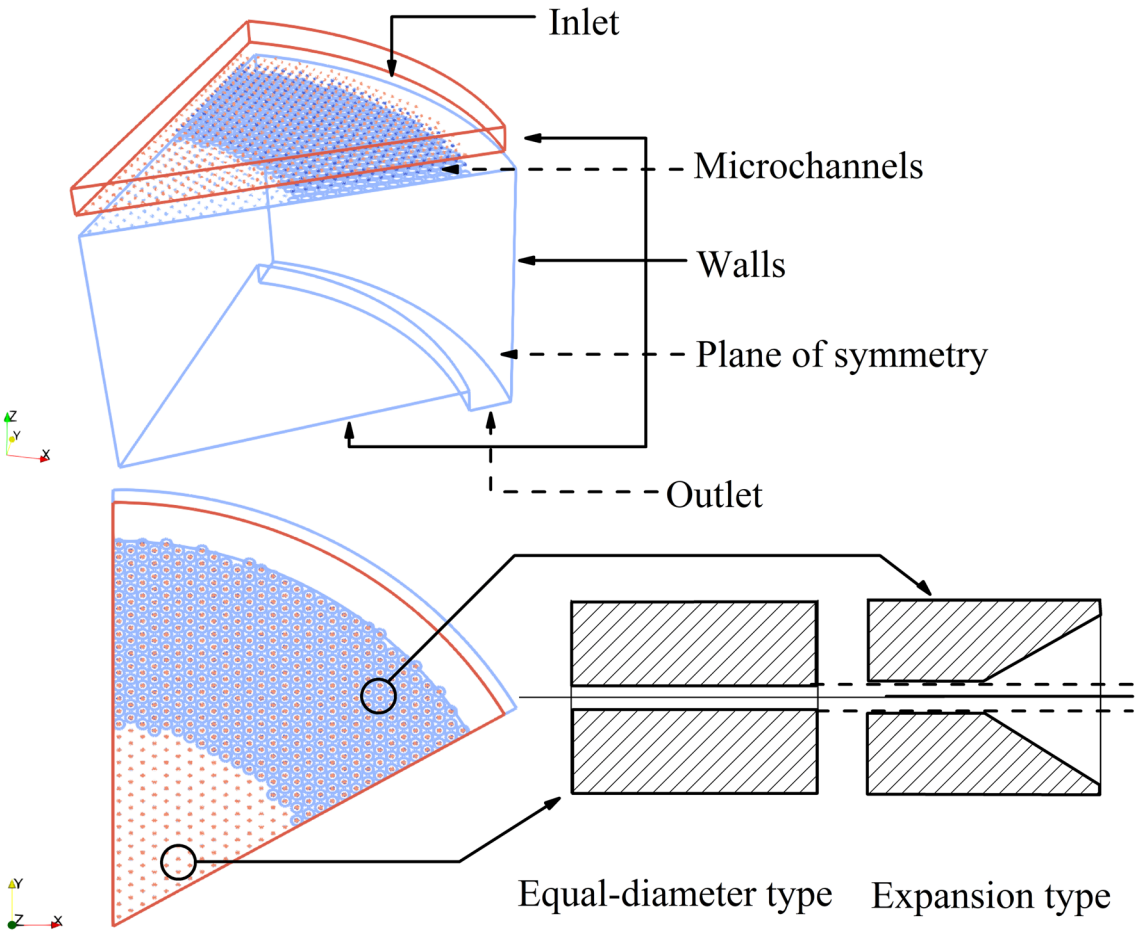

Fig. 8 Schematic diagram of simulation structure

direction for the equal-diameter type would be in all directions from the outlet.

To eliminate the differences caused by the flow rates of the two types of microchannels, we also analyzed the effect of flow resistance. The velocity of the equal-diameter type is used as the base. By decreasing the diameter of the expansion type, the flow resistance was increased. The 100% increase in flow resistance shown in Fig. 12 indicates that the expansion type got the same flow resistance as the equal-diameter type. It shows that the expansion type got a higher flow velocity, even when the flow resistance increased to 1.7 times that of the equal-diameter type.

Last but not least, it is important to ensure that the composite structure exhibits the same characteristics as the microchannel in different flow regimes. The microchannel composite structure is shown in Fig. 13. The flow in the chamber was simulated in both slip flow and transition flow regimes using the same structure. In the center of the chamber, the velocity in the slip flow regime was higher than that in the transition regime, and the velocity was higher in the transition flow regime at the edge of the chamber. This phenomenon was observed in the slip flow regime, where the equal-diameter type exhibited a stronger jet compared to the expansion type. However, this situation would reverse in the transition regime. The result is consistent with the flow characteristics of the single microchannel.

From the above, it can be seen that in PECVD production, when attempting to control the deposition distribution of the film using various types of microchannel combinations, it is essential to have a thorough understanding of the fluid regime. Under various flow regimes, the flow velocity varied significantly among different microchannels. The expected film thickness distribution can only be obtained through the correct microchannel distribution. Otherwise, a significantly different distribution might result.

The expansion type microchannel exhibited a significantly higher velocity than the equal-diameter types in the transition regime. The expansion type should be placed in the center of the PECVD chamber, while the equal-diameter type should be placed at the edge. In this way, the velocity difference between the central area and the edge can

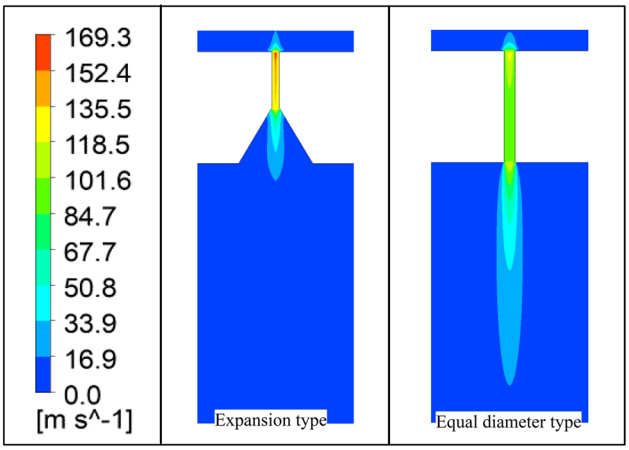

(a)

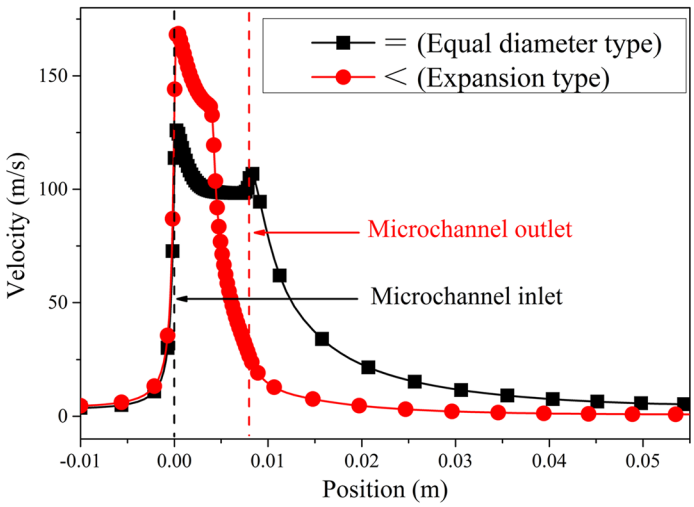

(b)

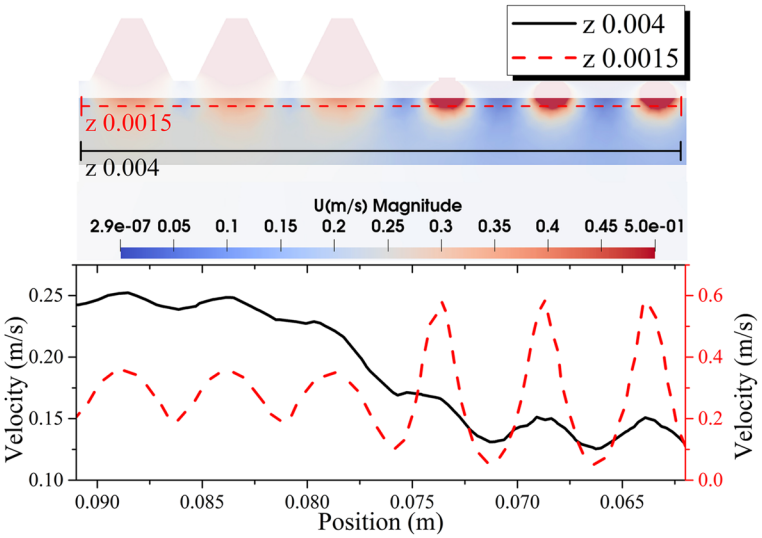

(c)

Fig. 9 Microchannel jet velocity contours and curves, **a** slip flow region contours, **b** slip flow region axial velocity curves, **c** transition flow region contour and curves

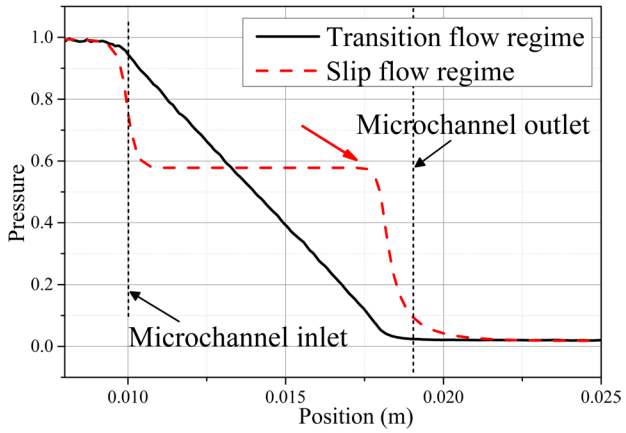

Fig. 10 Pressure distributions of slip flow and transition flow in equal-diameter type microchannels

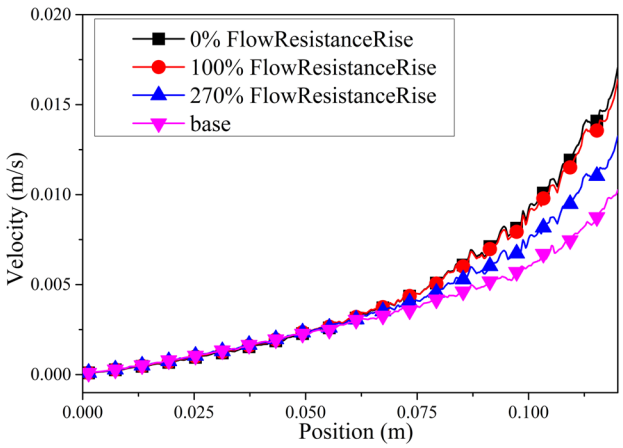

Fig. 12 Comparison of the velocity distribution of the expansion type and the equal-diameter type under different flow resistances

be reduced, thereby improving the uniformity of the film thickness.

5 Conclusion

In this paper, the NS-DSMC method, which is commonly used for return capsule and micro-thruster plume analysis in near-Earth space, is applied to calculate the flow field in PECVD. Different from other PECVD flow field calculations that use continuum flow methods, the NS-DSMC method can accurately obtain the gas flow characteristics in the transition regime or molecular state within the microchannel on the showerhead, as well as its jet characteristics. This is of great significance for PECVD processes that are sensitive to flow field effects.

We also adopted a two-way coupling approach in our study. Different from the conventional one-way coupling method, the data in the two-way coupling method will be transmitted bidirectionally between the NS and DSMC modules. This allows for simultaneous updates of the two calculation domains, resulting in improved calculation efficiency. The NS-DSMC coupling method matches the results of the DSMC method and is consistent with the experimental findings.

Fig. 11 Horizontal distribution of jet velocity

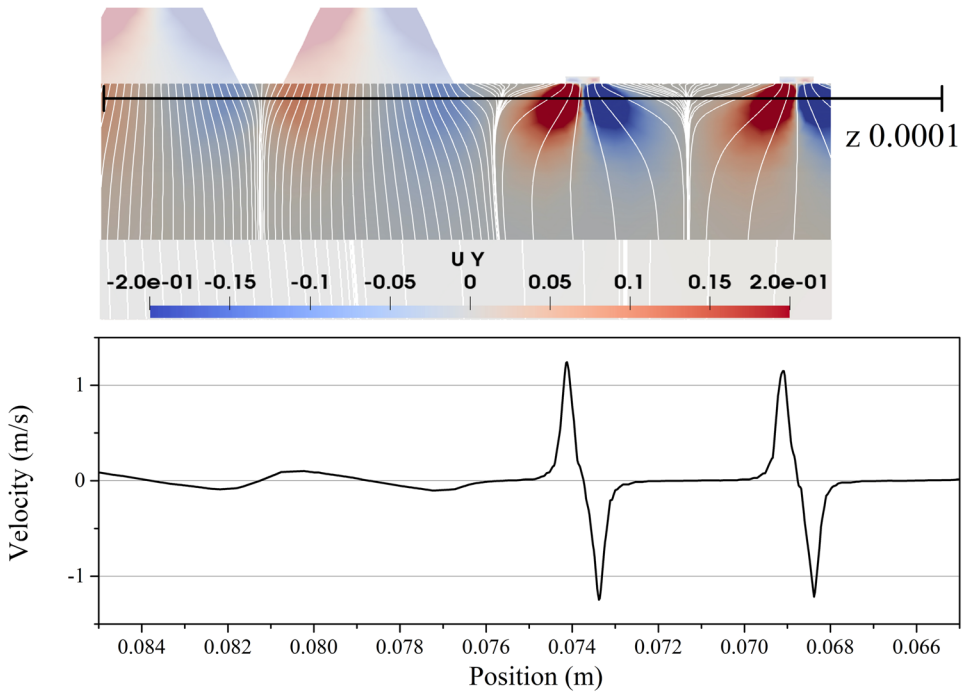

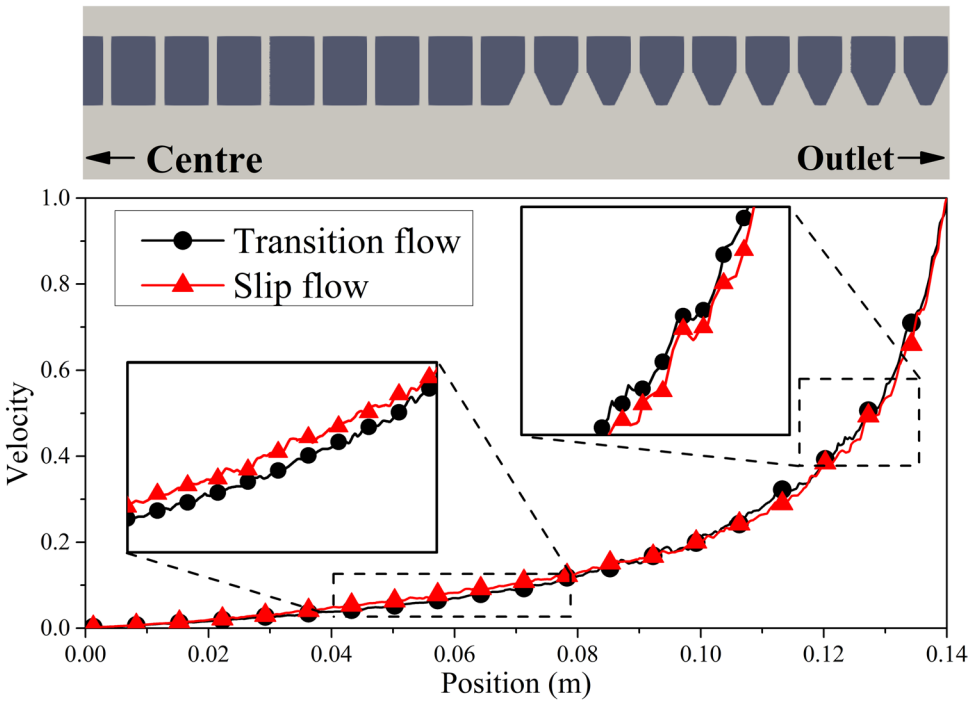

Fig. 13 Velocity distribution curves in slip flow and transition flow regimes with the same microchannel distribution at 1 mm above the wafer

By comparing the microchannel jet data under different flow regimes, we found that the fluid regime influences the pressure distribution in the microchannel, which in turn affects the jet characteristics of the microchannel. The equal-diameter type exhibits a higher jet velocity in the continuum regime. In the transition regime, the expansion type microchannel has a higher velocity. Therefore, the design of the showerhead microchannel needs to be compatible with the process environment. Different fluid regimes can result in variations in velocity distribution and cause changes in the thickness of the deposited film.

In addition, when using a combination of various microchannels, it is recommended to place the type with higher velocity in the central area and the type with lower velocity on the edge. This arrangement helps to minimize the difference in flow velocity between the center and the edge, resulting in improved deposition uniformity. Different from other methods of altering the length of the microchannel, the flow rate can be adjusted by enlarging the size of the outlet. This could potentially be a new approach for improving showerhead functionality.

The NS-DSMC method used in this paper is not a state-of-the-art adaptive boundary method. The adaptive boundary method can automatically determine the coupling position based on the distribution of the flow field, instead of using a pre-specified position as adopted in this paper. In this paper, the method of pre-specified coupling position serves two purposes. One purpose is to facilitate the establishment of two-way coupling, while the other purpose is to serve as the foundation for establishing a unified coupling method in the future. Using the two-way coupling and unified coupling methods can greatly improve the calculation efficiency of the showerhead flow field.

Author contributions Wansuo Liu (First Author): Conceptualization, Data Curation, Formal Analysis, Investigation, Resources, Methodology, Software, Validation, Writing - Original Draft; Xiangji Yue: Methodology, Project Administration, Software, Validation; Zeng Lin (Corresponding Author): Conceptualization, Funding Acquisition, Resources, Supervision, Writing - Review & Editing.

Funding This work was supported by National Natural Science Foundation of China [grant numbers 51775096]; Chinese Academy of Sciences WEGO Research Development Plan [grant numbers [2007]006]; and Fundamental Research Funds for the Central Universities, China [grant numbers N2003009].

Data availability The authors confirm that the data supporting the findings of this study are available within the article. Raw data that support the findings of this study are available from the corresponding author, upon reasonable request.

Declarations

Conflict of interest The authors declare no competing interests.

References

Aktas O, Aluru NR (2002) A combined continuum/DSMC technique for multiscale analysis of microfluidic filters. J Comput Phys 178(2):342–372. https://doi.org/10.1006/jcph.2002.7030

Aktas O, Aluru NR, Ravaioli U (2001) Application of a parallel DSMC technique to predict flow characteristics in microfluidic filters. J

Microelectromech Syst 10(4):538–549. https://doi.org/10.1109/84.967377
Arkilic EB, Schmidt MA, Bruer KS (1997a) Measurements of the TMAC in silicon microchannels. Rarefied gas dynamics. Peking University Press, p 983
Arkilic EB, Schmidt MA, Breuer KS (1997b) Gaseous slip flow in long microchannels. J Microelectromech Syst 6(2):167–178. https://doi.org/10.1109/84.585795
Beskok A, Karniadakis GE, Trimmer W (1996) Rarefaction and compressibility effects in gas microflows. Fluids Eng 118(3):448–456. https://doi.org/10.1115/1.2817779
Bird GA (1976) Molecular gas dynamics. NASA STI/Recon Tech Rep A 76:40225
Cai G, Liu L, He B et al (2022) A review of research on the vacuum plume. Aerospace 9(11):706. https://doi.org/10.3390/aerospace9110706
Eggers J, Beylich AE (1994) New algorithms for application in the direct simulation Monte Carlo method. Rarefied Gas Dyn Theory Simul 19:166–173
Fan J, Shen C (2001) Statistical simulation of low-speed rarefied gas flows. J Comput Phys 167(2):393–412. https://doi.org/10.1006/jcph.2000.6681
Farber K, Farber P, Gräbel J et al (2016) Development and validation of a coupled Navier–Stokes/DSMC simulation for rarefied gas flow in the production process for OLEDs. Appl Math Comput 272:648–656. https://doi.org/10.1016/j.amc.2015.05.040
Gad-el-Hak M (1999) The fluid mechanics of microdevices—the Freeman scholar lecture. J Fluids Eng 121(1):5–33. https://doi.org/10.1115/1.2822013
Gao R, O'Byrne S, Liow JL et al (2018) An experimental study of pressure distribution nonlinearity in a circular micro-tube. Exp Thermal Fluid Sci 97:468–483. https://doi.org/10.1016/j.expthermflusci.2018.05.020
Ghazanfari V, Shademan MM, Mansourzadeh F (2022) Investigation of feed flow effect using CFD-DSMC method in a gas centrifuge. J Nucl Res Appl 2(4):7–14. https://doi.org/10.24200/jon.2022.1027
Huang CY, Lai CM (2012) Pressure measurements with molecule-based pressure sensors in straight and constricted PDMS microchannels. J Micromech Microeng 22(6):065021. https://doi.org/10.1088/0960-1317/22/6/065021
Jang J, Wereley ST (2004) Pressure distributions of gaseous slip flow in straight and uniform rectangular microchannels. Microfluid Nanofluid 1(1):41–51. https://doi.org/10.1007/s10404-004-0005-8
John B, Damodaran M (2009) Hybrid continuum–direct simulation Monte Carlo and particle-laden flow modeling in the head-disk interface gap. IEEE Trans Magn 45(11):4929–4932. https://doi.org/10.1109/TMAG.2009.2029390
Kim HJ, Lee HJ (2017) Effects of the wall boundary conditions of a showerhead plasma reactor on the uniformity control of RF plasma deposition. J Appl Phys 122(5):053301. https://doi.org/10.1063/1.4996998
Ko HS, Gau C (2011) Local heat transfer process and pressure drop in a micro-channel integrated with arrays of temperature and pressure sensors. Microfluid Nanofluid 10(3):563–577. https://doi.org/10.1007/s10404-010-0690-4
Lee G, Sohn DK, Seok SH et al (2019) The effect of hole density variation in the PECVD reactor showerhead on the deposition of amorphous carbon layer. Vacuum 163:37–44. https://doi.org/10.1016/j.vacuum.2019.02.009
Moss JN, Price JM (1997) Survey of blunt body flows including wakes at hypersonic low-density conditions. J Thermophys Heat Transfer 11(3):321–329. https://doi.org/10.2514/2.6252
Palharini RC, White C, Scanlon TJ et al (2015) Benchmark numerical simulations of rarefied non-reacting gas flows using an open-source DSMC code. Comput Fluids 120:140–157. https://doi.org/10.1016/j.compfluid.2015.07.021
Pong KC, Ho CM, Liu J et al (1994) Non-linear pressure distribution in uniform microchannels. ASME-Publications-FED 197:51–51
Rafi KMM, Deepu M, Rajesh G (2019) Effect of heat transfer and geometry on micro-thruster performance. Int J Therm Sci 146:106063. https://doi.org/10.1016/j.ijthermalsci.2019.106063
Roveda R, Goldstein DB, Varghese PL (1998) Hybrid Euler/particle approach for continuum/rarefied flows. J Spacecr Rocket 35(3):258–265. https://doi.org/10.2514/2.3349
Roveda R, Goldstein DB, Varghese PL (2000) Hybrid Euler/direct simulation Monte Carlo calculation of unsteady slit flow. J Spacecr Rocket 37(6):753–760. https://doi.org/10.2514/2.3647
Scanlon TJ, Roohi E, White C et al (2010) An open source, parallel DSMC code for rarefied gas flows in arbitrary geometries. Comput Fluids 39(10):2078–2089. https://doi.org/10.1016/j.compfluid.2010.07.014
Schwartzentruber TE, Boyd ID (2006) A hybrid particle-continuum method applied to shock waves. J Comput Phys 215(2):402–416. https://doi.org/10.1016/j.jcp.2005.10.023
Sun Q, Boyd ID (2005) Evaluation of macroscopic properties in the direct simulation Monte Carlo method. J Thermophys Heat Transfer 19(3):329–335. https://doi.org/10.2514/1.12542
Virgile C, Albert A, Julien L (2022) Optimisation of a hybrid NS–DSMC methodology for continuous–rarefied jet flows. Acta Astronaut 195:295–308. https://doi.org/10.1016/j.actaastro.2022.03.012
Wagner W (1992) A convergence proof for Bird's direct simulation Monte Carlo method for the Boltzmann equation. J Stat Phys 66:1011–1044. https://doi.org/10.1007/BF01055714
Weng CI, Li WL, Hwang CC (1999) Gaseous flow in microtubes at arbitrary Knudsen numbers. Nanotechnology 10(4):373. https://doi.org/10.1088/0957-4484/10/4/302
Wi SS, Kim YG, Lee HJ et al (2012) Effects of showerhead hole structure on the deposition of hydrogenated microcrystalline silicon thin films by vhf PECVD. J Vac Sci Technol A 30(4):04D113. https://doi.org/10.1116/1.4721287
Xiang D, Xia H, Yang W et al (2019) Parametric study and residual gas analysis of large-area silicon-nitride thin-film deposition by plasma-enhanced chemical vapor deposition. Vacuum 165:172–178. https://doi.org/10.1016/j.vacuum.2019.04.017
Yambe K, Taka S, Ogura K (2014) Relation between plasma plume density and gas flow velocity in atmospheric pressure plasma. Phys Plasmas 21(4):043511. https://doi.org/10.1063/1.4873384
Yuan Z, Zhao W, Jiang Z et al (2020) Modified nonlinear coupled constitutive relations model for hypersonic nonequilibrium flows. J Thermophys Heat Transfer 34(4):848–859. https://doi.org/10.2514/1.T5761
Zohar Y, Lee SYK, Lee WY et al (2002) Subsonic gas flow in a straight and uniform microchannel. J Fluid Mech 472:125–151. https://doi.org/10.1017/S0022112002002203